

PCCP

Accepted Manuscript



This is an *Accepted Manuscript*, which has been through the Royal Society of Chemistry peer review process and has been accepted for publication.

Accepted Manuscripts are published online shortly after acceptance, before technical editing, formatting and proof reading. Using this free service, authors can make their results available to the community, in citable form, before we publish the edited article. We will replace this *Accepted Manuscript* with the edited and formatted *Advance Article* as soon as it is available.

You can find more information about *Accepted Manuscripts* in the [Information for Authors](#).

Please note that technical editing may introduce minor changes to the text and/or graphics, which may alter content. The journal's standard [Terms & Conditions](#) and the [Ethical guidelines](#) still apply. In no event shall the Royal Society of Chemistry be held responsible for any errors or omissions in this *Accepted Manuscript* or any consequences arising from the use of any information it contains.

ARTICLE

Predicting paramagnetic ^1H NMR chemical shifts and state-energy separations in spin-crossover host-guest systems

Cite this: DOI: 10.1039/x0xx00000x

Received 00th January 2012,
Accepted 00th January 2012

DOI: 10.1039/x0xx00000x

www.rsc.org/

William C. Isley III,^a Salvatore Zarra,^b Rebecca K. Carlson,^a Rana A. Bilbeisi,^b Tanya K. Ronson,^b Jonathan R. Nitschke,^{b*} Laura Gagliardi,^{a*} and Christopher J. Cramer^{a*}

The behaviour of metal-organic cages upon guest encapsulation can be difficult to elucidate in solution. Paramagnetic metal centres introduce additional dispersion of signals that is useful for characterisation of host-guest complexes in solution using nuclear magnetic resonance (NMR). However, paramagnetic centres also complicate spectral assignment due to line broadening, signal integration error, and large changes in chemical shifts, which can be difficult to assign even for known compounds. Quantum chemical predictions can provide information that greatly facilitates the assignment of NMR signals and identification of species present. Here we explore how the prediction of paramagnetic NMR spectra may be used to gain insight into the spin crossover (SCO) properties of iron(II)-based metal organic coordination cages, specifically examining how the structure of the local metal coordination environment affects SCO. To represent the tetrahedral metal-organic cage, a model system is generated by considering an isolated metal-ion vertex: *fac*- ML_3^{2+} ($\text{M} = \text{Fe}^{\text{II}}, \text{Co}^{\text{II}}$; $\text{L} = \text{N-phenyl-2-pyridinaldimine}$). The sensitivity of the ^1H paramagnetic chemical shifts to local coordination environments is assessed and utilised to shed light on spin crossover behaviour in iron complexes. Our data indicate that expansion of the metal coordination sphere must precede any thermal SCO. An attempt to correlate experimental enthalpies of SCO with static properties of bound guests shows that no simple relationship exists, and that effects are likely due to nuanced dynamic response to encapsulation.

Introduction

Paramagnetic nuclear magnetic resonance (NMR) spectroscopy can be a useful tool for assessing the structure and speciation of high-spin transition-metal coordination compounds in the solid state and solution.¹⁻⁷ In the case of proton-bearing organic ligands coordinating to a high-spin centre, the sensitivity of ^1H chemical shifts to the distance of individual protons from the paramagnetic nucleus makes this spectroscopic technique well-suited for the evaluation of small structural differences that take place in molecules as a result of an external stimulus, for example, the variation in structure of a metal-organic host that might occur following complexation of a suitable guest.⁸

A reliable magnetic indicator for guest binding would be a valuable tool for studying spin crossover (SCO) phenomena in solution and the solid state, indeed this concept has been applied to study anion complexation to metal receptors.^{9, 10} One desirable magnetic response to guest encapsulation would be the transition from a diamagnetic state to a paramagnetic state (or vice versa), as demonstrated by Ono *et al.*, where a Ni^{II} -

containing guest changes spin state upon encapsulation.¹¹ If the spin crossover was to occur in the host upon encapsulation, one could perform a variety of host-guest studies, followed by the magnetic transition. Given that iron(II) has been the focus of many single molecule or nanocrystalline magnet studies,¹²⁻²⁶ and that iron(II) is a fundamental component of many host complexes,²⁷ an exploration of the influence of guest encapsulation on an iron(II)-based host complex is a natural next step. Since the Fe(II) SCO phenomena typically involves a change in iron-ligand distances due to changes in electronic structure,^{28, 29} guest complexation might be leveraged to alter SCO behaviour.

For a species with a diamagnetic ground state and thermally accessible paramagnetic state, the temperature-dependent paramagnetic chemical shift will depend on the spin crossover energy. It has been shown in the literature for density functional methods that the functional choice, and especially the amount of exact Hartree-Fock (HF) exchange, can greatly affect the predicted spin crossover energetics of iron(II) complexes.³⁰⁻³⁷

Wave function theory *ab initio* methods, including CASPT2, can be extremely demanding in terms of computational resources but can also produce more accurate results when applied in a fashion that takes advantage of their systematic improvability.^{38, 39}

While spectroscopic data are sufficient to make general inferences with respect to relative separations of magnetic nuclei, the combination of paramagnetic NMR spectroscopy and quantum chemical calculations offers the opportunity to gain further insights at the molecular level of detail. Indeed, spectroscopy and computational predictions have been used in conjunction to investigate spin crossover (SCO) complexes previously.⁴⁰⁻⁴² In the present work we assess the accuracy of a particular density functional protocol for the prediction of ¹H chemical shifts in iron(II) and cobalt(II) coordination compounds analogous to those known to be useful as vertices for metal-templated self-assembled molecular cages.^{22, 43} The sensitivity of the chemical shifts to local structural changes and the utility of the DFT protocol for interpreting spin-crossover behaviour in iron-based systems are also examined. Given the importance of predicting an accurate high-spin (HS) – low-spin (LS) splitting energy ($\Delta E_{\text{HS-LS}}$) and that $\Delta E_{\text{HS-LS}}$ are notoriously difficult to predict for iron spin crossover complexes (SCO),³¹ special emphasis is placed on benchmarking and characterising methodological dependence on $\Delta E_{\text{HS-LS}}$ as a function of the coordination environment.

Results and discussion

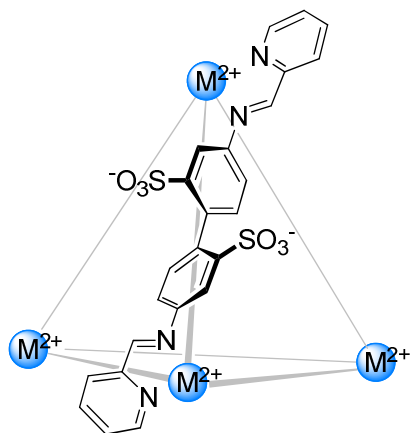
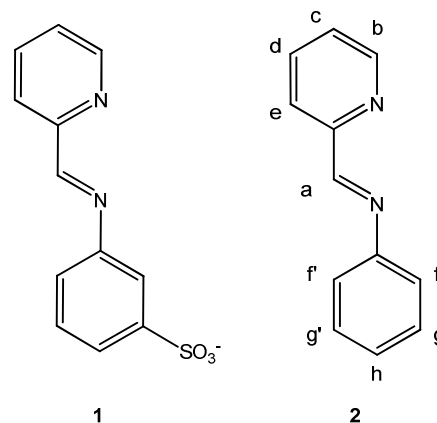


Figure 1. Sulfonated tetrahedral $[M_4L_6]^{4+}$ cage, where $M = \text{Co}^{\text{II}}$ (A) or Fe^{II} (B). Each edge of the tetrahedron represents the bis-bidentate ligand L shown.

Cobalt(II). We begin by considering the tetrahedral $[M_4L_6]^{4+}$ cobalt-based cage A⁴⁴ shown in Figure 1. This tetrahedral cage with sulfonated ligands has been synthesised with other metal cations such as iron, and nickel.^{27, 44} The solution-state ¹H NMR spectroscopy and the X-ray characterisation of cage A were previously described.⁴⁴

As quantum chemical computations for the full cage A would be extremely demanding and likely multiconfigurational, and as the spin centres are expected to have negligible

communication over the distances that separate them,⁴⁵ we chose to model the mononuclear complex corresponding to a corner, namely, $[\text{Co}(\mathbf{1})_3]^{1-}$ and the non-functionalised analogue $[\text{Co}(\mathbf{2})_3]^{2+}$ (see Scheme 1 for ligand labelling and position numbering scheme). To benchmark the accuracy of the DFT paramagnetic NMR modelling protocol, a high-spin (HS) truncated cage corner model is compared to experimental chemical shift values measured for the cage A.



Scheme 1.

$[\text{Co}(\mathbf{1})_3]^{1-}$. The optimised structure for the high-spin quartet state of $[\text{Co}(\mathbf{1})_3]^{1-}$ has bond lengths of 2.19 and 2.15 Å averaged over the three equivalent bonds to the imine and pyridine nitrogen atoms, respectively. We note the presence of Jahn-Teller distortion in the optimised geometry. The high-spin quartet state is the only state we have observed *in situ* for cobalt(II) tris(pyridylimine) complexes,^{44, 46} and the calculated $[\text{Co}(\mathbf{1})_3]^{1-}$ structure compares favourably with experimentally-observed structural features of cage A. The X-ray crystal structure of cage A with encapsulated tetrahydrofuran (THF)⁴⁴ exhibits average Co–N distances of 2.15 and 2.13 Å between imine and pyridine N atoms, respectively.

The ¹H NMR chemical shifts for the optimised quartet structure of $[\text{Co}(\mathbf{1})_3]^{1-}$ are presented in Table 1. Due to the presence of Jahn-Teller distortion that breaks the C_3 symmetry, the computed ¹H chemical shifts differ for equivalent protons on each linker. Under the assumption that thermal interconversion between equivalent minima will be rapid, we average the chemical shifts for equivalent protons as described in the experimental section. Here we note that the imine (H_a) and py-6 (H_b) protons exhibit the chemical shifts that are most sensitive to the paramagnetic centre. For all Co^{II} systems, predicted H_b chemical shift values were much larger than the experimentally measured ones. Neither increasing the H_b distance from the paramagnetic centre, nor the inclusion of explicit solvent molecules, yielded an improved agreement of the H_b chemical shift with the experimental shift. This significant over prediction has been observed by Rastrelli *et al.* for the $S=1$ $[\text{Ni}(\text{py})_6]^{2+}$ system.⁴⁷

Paramagnetic NMR predictions reported in the literature tend to overestimate observed chemical shifts;⁴⁸ thus, scaling of

Table 1. B3LYP chemical shifts for $[\text{Fe}(\mathbf{2})_3]^{2+}$ structure for all spin multiplicities, $[\text{Co}(\mathbf{1})_3]^{1-}$, $[\text{Co}(\mathbf{2})_3]^{2+}$ and experimental ^1H chemical shifts for the cage \mathbf{A}^{44} analogous to $\text{Co}(\mathbf{1})_3^{1-}$. All chemical shifts are reported in ppm.

^1H Position ^a	Experimental Co^{II}			Predicted Co^{II}			Predicted Fe^{II}				
	Solvated \mathbf{A} S=3/2 $\delta_{\text{exp}}^{b,e}$	Guest $\mathbf{C} \subset \mathbf{A}$ S=3/2 $\delta_{\text{exp}}^{b,e,f}$	$[\text{Co}(\mathbf{2})_3]^{2+}$ S=3/2 $\delta_{\text{exp}}^{b,g}$	$[\text{Co}(\mathbf{1})_3]^{1-}$ S=3/2 $\delta_{\text{fit}}^{b,c,d}$	$[\text{Co}(\mathbf{2})_3]^{2+}$ S=3/2 $\delta_{\text{fit}}^{b,c,d}$	S=0 $\delta^{b,c}$	S=1 $\delta_{\text{fit}}^{b,c,d}$	$[\text{Fe}(\mathbf{2})_3]^{2+}$			S=2 \mathbf{Q}_3 $\delta_{\text{fit}}^{b,c,d,f}$
								S=2 \mathbf{Q}_1 $\delta_{\text{fit}}^{b,c,d,h}$	S=2 \mathbf{Q}_2 $\delta_{\text{fit}}^{b,c,d,i}$	S=2 \mathbf{Q}_3 $\delta_{\text{fit}}^{b,c,d,j}$	
H _a (Imine-C)	244.0	238.2	240.6	251.3	247.0	9.4	68.2	244.5	247.4	259.4	
H _b (Py-6)	88.6	88.6	88.5	155.8	172.9	8.2	61.5	175.9	167.2	167.0	
H _c (Py-5)	74.3 ^k	74.9 ^k	74.0 ^k	50.0	56.6	8.2	23.8	63.5	65.3	62.0	
H _d (Py-4)	17.1	17.1	16.6	15.8	19.8	8.9	21.1	18.2	16.6	10.1	
H _e (Py-3)	52.8 ^k	52.8 ^k	52.4 ^k	47.5	52.0	9.0	17.0	59.8	56.4	61.4	
H _f (Phe-2)	-7.6 ^k	-5.7 ^k	-21.2	-12.8	-12.8	6.6	-3.8	-10.9	9.4	-10.8	
H _f (Phe-2')	-44.0 ^k	-41.6 ^k	-21.2	-15.4	-25.4	4.6	-5.7	-21.9	-7.8	-10.2	
H _g (Phe-3)	--	--	10.1	--	11.6	7.8	6.5	12.2	13.7	14.4	
H _{g'} (Phe-3')	20.5	20.5	10.1	18.3	23.4	7.6	7.9	21.3	16.2	19.1	
H _h (Phe-4)	--	--	-12.0	-10.8	-15.8	8.0	-2.4	-14.4	-4.6	-7.9	

^a See Scheme 1 for position labelling. Values are averages over the three chemically equivalent positions in the complex. ^b Relative to TMS. ^c Computed for mononuclear cage corner model. ^d Rescaled chemical shifts according to linear regression $\delta_{\text{fit}} = 0.9790(\delta_{\text{pred}}) - 4.02$. ^e Measured for \mathbf{A}^{44} . ^f Measured for \mathbf{A} with bound 2-pyridinecarboxaldehyde. ^g Measured for $[\text{Co}(\mathbf{2})_3]^{2+}$. Chemical shifts for the *facial* isomer are listed. ^h Quintet structure \mathbf{Q}_1 . ⁱ Quintet structure \mathbf{Q}_2 . ^j Quintet structure \mathbf{Q}_3 . ^k Based on the comparison between theory and experiment, the experimental assignments of the two ^1H pairs (py-3 / py-5) and (phe-2 / phe-2') are swapped.

predicted chemical shifts to match experimental measurements should yield a model with improved predictive abilities. A linear regression (plotted in Figure S1) of the predicted chemical shifts for $[\text{Co}(\mathbf{1})_3]^{1-}$ on the ^1H NMR spectra of the host cage \mathbf{A}^{44} yields $\delta_{\text{fit}} = 0.9790(\delta_{\text{pred}}) - 4.02$ with associated $R^2 = 0.9697$ (additional discussion of the linear regression is provided in the Supporting Information). The linear regression demonstrates that the current modelling protocol has remarkably good agreement with experimental measurements.

The average predicted value for H_a ^1H ($\delta_{\text{fit}} = 251.3$ ppm) is referenced to that measured for empty cage \mathbf{A} (244.0 ppm) and also comparable to cage \mathbf{A} encapsulating 2-pyridinecarboxaldehyde (238.2 ppm). Given the large paramagnetic shift, and its sensitivity to structural changes (*vide infra*), we consider the agreement within the range of previously reported differences between predicted and experimental ^1H δ .^{47, 49} It is noteworthy that upon experimental guest encapsulation, the imine proton signal shifts upfield. This is postulated to result from an expansion of the imine bond $^1\text{H} - \text{Co}$ distance upon guest encapsulation.

$[\text{Co}(\mathbf{2})_3]^{2+}$. A comparison of the predicted chemical shifts between the sulfonated model complex $[\text{Co}(\mathbf{1})_3]^{1-}$ and the unsubstituted model complex $[\text{Co}(\mathbf{2})_3]^{2+}$ indicates qualitative agreement. Given that the calculated NMR spectrum of $[\text{Co}(\mathbf{2})_3]^{2+}$ shows very close agreement with that of $[\text{Co}(\mathbf{1})_3]^{1-}$,⁴⁶ we studied the less complex model in the case of iron(II), with the neutral ligand $\mathbf{2}$ instead of the larger and anionic ligand $\mathbf{1}$.

Iron(II). Having assessed the quantitative utility of the computational model for the cobalt cage above, we turned next to iron-based systems. These are more difficult to treat in

practice than their Co^{II} congeners because at experimental temperatures more than one spin state may be thermally populated for the iron-based systems. Under such circumstances, spin crossover will lead to observation of NMR chemical shifts averaged over the states. The experimental ground state for Fe^{II} -containing cage \mathbf{B} is largely the singlet diamagnetic state, with a very small population of paramagnetic character affecting NMR spectra. We show below that the S=2 spin state is the most accessible paramagnetic state, and produces a paramagnetic shift that agrees with experimental spin crossover data.

$[\text{Fe}(\mathbf{2})_3]^{2+}$. The optimised structure for the low-spin singlet state of the $[\text{Fe}(\mathbf{2})_3]^{2+}$ complex has Fe–N bond lengths of 1.99 Å for both pyridine and imine nitrogen atoms, averaged over the three equivalent bonds of each type. These distances agree with experimentally measured bond distances from the X-ray crystal structure of the sulfonated cage²⁷ (1.986(6) Å and 1.972(5) Å, for the pyridyl and imine bonds respectively), and also reinforces the assumption that the local environment of the metal centre is accurately reproduced after truncation of the cage structure to a single corner.

The vertical triplet-singlet splitting at the singlet global minimum is computed to be 29.6 kcal mol⁻¹ at the CASPT2 level and 29.2 kcal mol⁻¹ at the M06-L level (see below for further comparison of spin-state energies as a function of computational protocol). Optimisation with M06-L along the S=1 potential energy surface leads to a local triplet minimum that is 16.8 kcal mol⁻¹ higher in free energy at the M06-L level than the S=0 ground state. As this large energy separation renders the triplet state effectively inaccessible to thermal

population at 298 K, we will not consider it further although predicted chemical shifts are provided in Table 1 for completeness.

The vertical $\Delta E_{\text{HS-LS}}$ associated with the quintet state at the singlet global minimum are computed to be 27.7 kcal mol⁻¹ at the CASPT2 level and 36.5 kcal mol⁻¹ at the M06-L level. Optimisation with the M06-L functional along the quintet potential energy surface leads to significant Jahn-Teller distortion and multiple local minima. These three minima, **Q**₁, **Q**₂, and **Q**₃, were found to have adiabatic $\Delta H_{\text{SCO}} = 7.7$ kcal mol⁻¹, 4.0 kcal mol⁻¹, and 3.7 kcal mol⁻¹, respectively, referenced to the singlet global minimum. For these three optimised spin state structures of [Fe(2)₃]²⁺, ¹H NMR chemical shifts are presented in Table 1. Other calculated properties for [Fe(2)₃]²⁺ are summarised in Table 2.

Table 2. Calculated Properties of the [Fe(2)₃]²⁺ structure for all spin multiplicities.

	S=0	S=1	Q ₁ S=2	Q ₂ S=2	Q ₃ S=2
ΔH_{SCO}^a	–	16.8	7.7	4.0	3.7
ΔG_{SCO}^a	–	14.4	4.2	1.3	0.9
Fe – N _{py} (Å)	1.99	2.08	2.17	2.21	2.19
Fe – N _{im} (Å)	1.99	2.08	2.20	2.18	2.21

^a Adiabatic transitions to the indicated spin state and geometry were computed at the M06-L level of theory for $T = 298$ K. Free energies and enthalpies of SCO, reported in kcal mol⁻¹, are referenced relative to the S=0 [Fe(2)₃]²⁺ global minimum energy structure.

Topological Influence of the Host. In order to simulate the possible topological influence of the cage **B** superstructure on $\Delta E_{\text{HS-LS}}$, the triangular base of the host tetrahedron's corner was modelled with the distance between the C_h Phe-4 carbon atoms on separate linkers fixed at the distance determined experimentally from X-ray crystallography. The average experimental inter-ligand Phe-4 C–C distance, as measured from cage **B**, is 6.3 ± 0.2 Å; this compares to an average distance of 5.7 Å on the optimised [Fe(2)₃]²⁺ structure. A constrained optimisation of [Fe(1)₃]²⁺ with each Phe-4 C – Phe-4 C' distance fixed at 6.3 Å yielded a splayed corner (SPC) structure. The free energy required to splay the corner from the ground state structure is predicted to be very small, $\Delta G_{\text{splay}} = 0.2$ kcal mol⁻¹. Splaying the corner reduces the vertical spin splitting by 2.1 kcal mol⁻¹, which demonstrates that splaying the corner has a small change in SCO properties. The computed vertical spin state splittings at the M06-L level are $\Delta E_{\text{HS-LS}}^{\text{SPC}} = 34.4$ kcal mol⁻¹ and $\Delta E_{\text{HS-LS}}^{\text{GS}} = 36.5$ kcal mol⁻¹.

Spin Crossover. Variation of the ¹H NMR chemical shifts for the resonances of host **B** and its host-guest complexes with temperature was measured by variable temperature (VT) ¹H NMR experiments (see Experimental Methods). In Figure 2 VT ¹H NMR data for the host-guest complex with cyclohexane, C₆H₁₂⊂**B**, are reported as a representative example. The protons H_a and H_b were observed to undergo the largest change in chemical shift with temperature due to their proximity to the metal centre (blue and red lines, respectively, in Figure 2). NMR chemical shifts affected by the spin crossover process have been modelled with Eqn. (1)^{41, 50}

$$\delta_{\text{obs}} = \delta_{\text{LS}} + \left(\frac{C}{T}\right) \frac{1}{1 + e^{\Delta G^{\circ}/RT}} \quad (1)$$

where δ_{obs} is the observed chemical shift, δ_{LS} is the low-spin chemical shift, C/T is, to first approximation, the chemical shift of the high-spin state δ_{HS} , T is the temperature, R is the gas constant, and ΔG° is the phenomenological free energy change for the low-spin to high-spin transition. This equation can be used to fit the VT ¹H NMR experiments and to extract thermodynamic information about the spin crossover process.

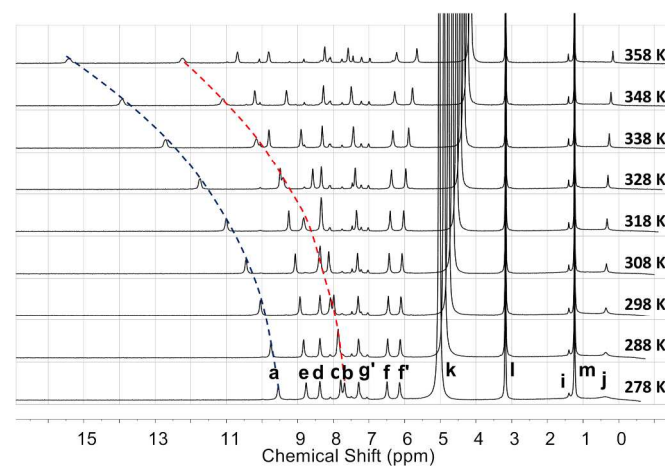


Figure 2. Stacked plot of ¹H NMR spectra for C₆H₁₂⊂**B** in D₂O acquired at temperatures from 278 (bottom) to 358 K (top) in 10 K steps. Lines are drawn to guide the eye to the changes in chemical shifts of protons H_a (depicted in blue) and H_b (depicted in red). Peak assignments for C₆H₁₂⊂**B** and for free C₆H₁₂ are also shown for the spectrum acquired at 278 K. a–g': protons are labelled in Scheme 2, i: free C₆H₁₂, j: bound C₆H₁₂, k: HDO, l: Me₄N⁺, m: *t*BuOH. At higher temperatures some of the cage (ca. 15% at 358 K) disassembled into its subcomponents through hydrolysis of the imine bonds. The minor peaks corresponding to subcomponents in each spectrum are left unlabelled for clarity.

The available experimental temperature range is limited by solvent properties and the degradation of cage **B** at high temperatures. As a result, the fully high-spin chemical shift cannot be obtained experimentally, so theoretical predictions of the chemical shift can be used to improve estimates for the spin crossover thermodynamics. Considering the imine proton, as it did not show any overlap with other signals in the VT NMR experiments, and using the computed values for δ_{HS} of the most stable quintet structure **Q**₃, fits for the model in Eqn. (1) to VT NMR data obtained from experiment yield ΔH_{SCO} values of 8.8 kcal mol⁻¹ and 7.0 kcal mol⁻¹ for the empty cage **B** and for **B** encapsulating cyclohexane, respectively. The results for SCO fits of VT imine ¹H NMR data are presented in Table 3 for these and several cases with other guests encapsulated. In each instance, the low-spin chemical shift (δ_{LS}) was taken to be 9.2 ppm as measured experimentally, and the high-spin chemical shift was taken to be 259.4 ppm, which is the theoretically predicted imine shift for the lowest energy quintet state. Further details concerning the fitting procedure can be found in the Supporting Information.

Guest Influence on Spin Crossover. As indicated in Table 3, guest binding impacts SCO behaviour; when examining the trends within chemical groups, one can observe trends in ΔH_{SCO} and ΔG_{SCO} . For example, increased Cl substitution on $\text{CH}_{4-x}\text{Cl}_x$ ($x=2,3,4$) shows an approximately 10% decrease in ΔG_{SCO} per Cl. Additionally, fluorination of benzene also shows a similar trend, where sequential substitution of F for H yields a sequential reduction in ΔG_{SCO} . However, these effects on SCO are quite small in absolute magnitude and we cannot reliably correlate these variations in SCO with changes in guest volume, polarizability or other guest properties.

We hypothesise that each guest induces a change in the local metal-ligand environment upon binding; however, multi-linear regression analysis to correlate physicochemical properties of the various guest molecules (*e.g.* volume, dipole moment, octanol-water partition coefficient, acidity or basicity) with ΔH_{SCO} did not yield any notable trends. Table S5 contains all physicochemical properties examined, as well as the enthalpy and entropy associated with spin crossover for the iron(II) cage with the listed encapsulated guest.

Table 3. ΔH_{SCO} and ΔS_{SCO} for the Fe^{II} singlet to quintet transitions as a function of encapsulated guests with the cage **B** depicted in Figure 1, fit from VT ^1H NMR measurements to Eqn. (1).

Guest	ΔH_{SCO}^a	ΔS_{SCO}^a	$\Delta G_{\text{SCO}} (T = 298 \text{ K})^a$
solvent ^b	8.8	14.9	4.4
acetone	6.6	10.7	3.4
tetrahydrofuran	7.0	11.6	3.6
cyclopentane	6.3	10.3	3.2
methylcyclopentane	4.6	7.3	2.4
pyridine	6.5	11.0	3.2
benzene	6.6	11.2	3.2
fluorobenzene	6.1	10.6	3.0
1,2-difluorobenzene	5.8	10.1	2.8
1,4-difluorobenzene	5.1	8.5	2.6
cyclohexane	7.0	12.2	3.4
1,4-dioxane	6.6	10.8	3.3
1,3,5-trioxane	8.4	14.8	4.0
CH_2Cl_2	7.6	12.4	3.9
CHCl_3	7.3	12.5	3.5
CCl_4	7.1	12.4	3.3

^a ΔH_{SCO} and ΔG_{SCO} are reported in kcal mol^{-1} . ΔS_{SCO} are reported in $\text{cal mol}^{-1} \text{K}^{-1}$. ^b The solvent used was water.

Functional Dependence. We performed a set of tests to improve our understanding of the sensitivity of predicted state-energy splittings to computational protocol, and to validate a practical density functional protocol in order to better survey structural influences on state-energy splittings. This testing was accomplished through a comparison of various density functional models with the more rigorous CASPT2 model for a series of molecular geometries expected to be relevant to a dynamical cage corner, namely, those associated with systematic variations in the $\text{Fe}-\text{N}_{\text{imine}}$ and $\text{Fe}-\text{N}_{\text{pyridine}}$ distances. Results are presented in Table 4. When compared to CASPT2 quintet-singlet state-energy splittings, OPBE exhibited the best performance over our 2D surface survey with a mean signed deviation (MSD) of $1.5 \text{ kcal mol}^{-1}$ and mean unsigned deviation (MUD) of $2.3 \text{ kcal mol}^{-1}$. Other density functionals that

performed reasonably well in comparison to the CASPT2 results were B3LYP with a MSD of $1.9 \text{ kcal mol}^{-1}$ and a MUD of $3.1 \text{ kcal mol}^{-1}$, M06-L with a MSD of $6.1 \text{ kcal mol}^{-1}$, a MUD of $6.1 \text{ kcal mol}^{-1}$, and B3LYP* with a MSD of $6.7 \text{ kcal mol}^{-1}$, a MUD of $6.7 \text{ kcal mol}^{-1}$.

The good performance of OPBE for the prediction of state-energy splittings in iron coordination compounds has been previously demonstrated for a number of compounds by Swart.³¹ We therefore anticipate that the OPBE predictions for the more expanded corner structures, where CASPT2 predictions become unreliable owing to active space limitations (a symptom of which is demonstrated by the increasingly large difference between the CAS and CASPT2 predicted energy separations), are likely to be the most reliable of those surveyed. M06-L tracks the OPBE predictions for the more expanded corners fairly well, making it a good choice for geometry optimisations that take computational advantage of its local character in these large systems.

B3LYP also tracks OPBE reasonably well for the less expanded corner geometries, but it predicts the quintet state to become the ground state at the largest Fe–N distances. B3LYP* is the only density functional with exact HF exchange that does not predict a quintet ground state at extended coordination shells. In every other case, density functionals containing more exact HF exchange predict an increasingly more stable quintet state. This is consistent with prior literature^{30,32} that have found a linear relationship between $\Delta E_{\text{HS-LS}}$ in iron complexes and the amount of exact exchange included in B3LYP calculations treating exact exchange as a variable, with an optimum functional form for iron $\Delta E_{\text{HS-LS}}$ at 15% exact exchange denoted B3LYP*.³²

Table 4. Functional survey of spin crossover electronic energy, $\Delta E_{\text{HS-LS}}$ (kcal mol^{-1}), on a 2D surface of symmetrically varied metal-ligand distances for $[\text{Fe}(\mathbf{2})_3]^{2+}$.

X: Fe-Py ^a	GS	2.00	2.00	2.10	2.10	2.10	2.20	2.20
Y: Fe-Im ^a	GS	2.00	2.10	2.00	2.10	2.20	2.10	2.20
CASSCF	20.0	13.6	-5.6	-3.2	^b	^b	^b	^b
CASPT2	27.7	24.4	16.7	16.1	^b	^b	^b	^b
B3LYP	33.9	28.2	15.0	15.5	4.4	-1.0	-0.6	-3.3
B3LYP+D3	33.9	29.6	18.5	19.2	9.9	1.1	2.2	-1.5
B3LYP*	38.2	32.7	20.3	20.5	10.3	5.7	5.7	3.6
O3LYP	26.8	20.5	7.8	7.3	-3.2	-7.9	-9.1	-10.4
M06-L	36.5	31.7	21.4	19.7	11.2	10.1	7.4	5.0
M06	5.6	0.9	-9.5	-9.7	-18.2	-21.0	-21.3	-23.4
M06-2X	-4.7	-9.5	-24.2	-22.5	-35.6	-42.4	-40.4	-47.0
PBE+D3	48.6	43.9	35.0	34.1	27.1	23.3	22.5	21.0
PBE	48.6	43.0	32.9	31.9	23.9	21.8	20.3	19.6
PBE0	20.1	15.2	3.7	4.1	-5.6	-9.7	-9.4	-12.0
OPBE	32.9	26.9	16.5	14.7	6.3	4.2	1.1	1.7

^a Distances are in Å between the metal centre and N atom indicated. GS indicates the unconstrained singlet ground state geometry. ^b In order to treat the expanded coordination system; an active space larger than (10,12) was found to be required, with which further calculations were not undertaken.

Inclusion of the empirical Grimme D3 dispersion correction with Becke-Johnson damping⁵¹ for B3LYP and PBE increases

the favourability of the more compact singlet ground state. This is consistent with previous observations in the literature of spin crossover complexes.³⁷

Dynamical Effects. Given that ΔH_{SCO} was predicted from the VT NMR data to be 8.8 kcal mol⁻¹ for the aqueous cage, and that the predicted *vertical* $\Delta E_{\text{HS-LS}}$ for the ground-state singlet geometry was 27.7 kcal mol⁻¹, we hypothesise that the observed thermal spin crossover must occur as part of a dynamical process. It is well established that high-spin iron(II) complexes have longer metal-ligand bonds than their low-spin counterparts due to the increased ionic radius of the high-spin metal,⁵² thus we also explored how systematic variation of Fe–N bond lengths reported in Table 4 for $[\text{Fe}(\mathbf{2})_3]^{2+}$ affects predicted paramagnetic chemical shifts, in addition to state-energy separation. Predicted ¹H chemical shifts for the quintet state of $[\text{Fe}(\mathbf{2})_3]^{2+}$ along the 2D surface are reported in Table S2.

Spatial variation in the Fe–N_{im} distance correlated strongly with variation in the paramagnetic chemical shift of the imine proton. On average, a 0.05 Å increase in Y, the Fe–N_{im} distance, resulted in a decrease in the imine ¹H δ of 38.0 ppm. However, variation in X, the Fe–N_{py} distance, did not strongly correlate with the computed imine ¹H chemical shift. On average, a 0.05 Å increase in Y results in a decrease in the imine ¹H δ of 0.2 ppm. Considering the sensitivity of the imine ¹H δ value to Fe–N_{im} distance, it is important to reconsider the data in Table 1, which were derived using a single value for imine ¹H δ taken from the lowest energy optimised quintet structure. However, if we vary the reference high-spin value from 220 to 280, the variation in the predicted thermodynamic variables of enthalpy and entropy is no more than 0.5% and 5%, respectively. This result indicates low sensitivity to the high-spin chemical shift endpoint in obtaining thermodynamic parameters for SCO using Equation (1).

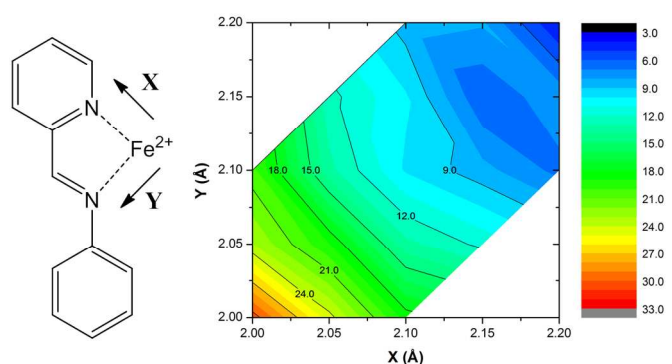


Figure 3. The M06-L state-energy splitting ΔH_{SCO} for $[\text{Fe}(\mathbf{2})_3]^{2+}$ between the singlet ground state structure and the quintet structure optimised with constrained, symmetrically frozen Fe–N bonds. Raw values can be found in the Supporting Information.

Figure 3 plots ΔH_{SCO} as a function of the two Fe–N coordinates. There is a large splitting energy at the ground-state geometry, which is quite close to the symmetrically constrained structure (2.00, 2.00). However, a sharp decrease in ΔH_{SCO} accompanies a slight expansion of the coordination sphere. The high-spin configuration is computed to be much more thermally

accessible upon expansion of the coordination sphere to (2.10, 2.10), with $\Delta H_{\text{SCO}} = 9.9$ kcal mol⁻¹. Indeed, this predicted ΔH_{SCO} agrees with the measured ΔH_{SCO} from VT NMR within experimental error. From these data, we conclude that spin crossover occurs for expanded corner structures, whose geometries are accessed dynamically at experimental temperatures.

Conclusions

In this work we have demonstrated the utility of quantum chemical models for the prediction of paramagnetic ¹H NMR chemical shifts in molecules incorporating high-spin metal centres. The predicted chemical shifts were consequently used for the prediction of thermodynamic parameters associated with spin-crossover (SCO) processes. We have further characterised how SCO can be affected by the geometrical expansion of the ligand sphere around Fe^{II} centres. A quantum mechanical survey of spin-state energy splittings suggests that SCO does not occur for molecular geometries near that of the singlet ground state, at which very large state-energy separations are predicted for pyridylimine-based Fe^{II} complexes. However, expansion of the metal coordination sphere reduces ΔH_{SCO} to the point that a high-spin quintet state becomes thermally accessible. This indicates that dynamical access to an expanded metal coordination sphere is necessary for spin crossover. Based on this conclusion, any guest molecule whose encapsulation serves to expand this coordination sphere, or otherwise stabilise the high-spin state, should result in increased high-spin population at a given temperature. We have explored whether variations in ΔH_{SCO} values measured experimentally for different guest molecules correlate with physicochemical properties of the guests themselves, but satisfactory correlations have not been identified. This suggests that the effects of guest binding on SCO properties are more nuanced than may be inferred from static calculations and that further insights will be likely to require dynamical simulations of host-guest complexes in solution and analysis of associated trajectories.

Experimental

Computational Methods.

Optimisation and Thermochemistry. Geometry optimisations were performed for all species at the M06-L⁵³ level of density functional theory. For Fe and Co atoms, the Stuttgart-Dresden (SDD) ECP10MDF [8s7p6d2f | 6s5p3d2f] basis set and associated pseudopotentials^{54, 55} were used; the MIDI! basis⁵⁶ was used for C, N, and H atoms; the 6-31+G(d) basis was used for S and O atoms. The nature of stationary points was assessed in all cases by computation of analytic vibrational frequencies, which were also used to compute the molecular partition functions necessary to predict 298 K thermochemical quantities using the conventional ideal-gas, rigid-rotator, quantum-mechanical quasi-harmonic-oscillator⁵⁷ approximation.⁵⁸ Improved electronic energies were computed, as single-point

calculations, using the same SDD basis set for Fe and Co but replacing MIDI! or 6-31+G(d), with 6-311+G(2df,p) for all other atoms.

Spin State Separations. Spin state splitting energies were computed at the CASSCF/PT2 level of theory with a (10,12) active space. Further details on these calculations are in the Supporting Information. In addition, several functionals were compared to the CASSCF/PT2 splitting energies including M06-L, M06, M06-2X, PBE, PBE0, B3LYP, B3LYP* O3LYP, and OPBE. The basis set used for these computations was the same as for the improved electronic energies as stated above.

Paramagnetic NMR. For isotropic systems 3d metal systems,^{6, 47, 49, 59, 60} the Fermi contact term is presumed to massively dominate the paramagnetic component of the chemical shift. For further discussion on the nature of the approximations made when computing the paramagnetic chemical shift, please see the Supporting Information. Thus the computed absolute chemical shift becomes

$$\sigma^{iso} = \sigma_{orb}^{iso} - \frac{S(S+1)}{3k_B T} \frac{2\pi\mu_B}{\gamma} g_{iso} A_{FC} \quad (2)$$

where γ is the gyromagnetic ratio for nucleus K , g_{iso} is the isotropic g -factor, μ_B is the Bohr magneton, A_{FC} is the isotropic hyperfine coupling constant (Fermi Contact HFC) for nucleus K in frequency units (multiply by \hbar if the HFC is in energy units), S is the electronic total spin, k_B is Boltzmann's constant, and T is temperature. σ_{orb}^{iso} is computed, approximately for high spin systems, on the unrestricted system using the diamagnetic formulation for the orbital shielding.⁶¹ The contribution to the orbital chemical shielding introduced by the additional "paramagnetic orbital shielding" term⁶² is expected to be small for ^1H nuclei, and is not computed in this work. Since σ_{iso} is an absolute chemical shielding, the observable chemical shift becomes

$$\delta = \sigma_{ref} - \sigma_{iso} \quad (3)$$

where σ_{ref} is the chemical shift of a reference compound, tetramethylsilane (TMS). Before computing δ_{pred} , σ_{orb} and A_{FC} are averaged for equivalent proton groups.

^1H chemical shifts δ , referenced to tetramethylsilane (TMS), were computed at the B3LYP level of DFT employing the all-electron 6-311+G basis set^{63, 64} for the metal atoms and the EPR-II basis⁶⁵ for C, N, H, O and the 6-311+G(2df) basis^{66, 67} for S. We chose to use the B3LYP functional based on previously demonstrated good NMR and EPR performance for metal-containing systems like those studied here.⁴⁷

Hyperfine coupling constants and the g -tensor were computed using the DFT level of theory in gas phase within the spin orbit mean field approximation SOMF(1X).⁶⁸ The extension for systems with $S > 1/2$ using the zero-field splitting interaction is neglected in this work; further discussion on this interaction and its effects on paramagnetic NMR are in the Supporting Information.

Solvation and Software. All optimisation, thermochemistry and σ_{orb} computations were accomplished using the

Gaussian09 Rev C.01 suite of electronic structure programs.⁶⁹ In all calculations with the Gaussian09 software suite, the effects of aqueous solvation were included using the SMD continuum solvation model.⁷⁰ All EPR computations were accomplished in the gas phase using the ORCA 2.9.1 suite⁷¹ of electronic structure programs.

Experimental Methods.

Variable Temperature ^1H NMR. Solutions of host cage **B** and its host-guest complexes were prepared as described in the Supporting Information. VT NMR experiments were performed using an automated temperature ramp which consisted of going from 278 K to 358 K in steps of 10 K. After each temperature was reached, 3 minutes for the equilibration of the sample were allowed and a ^1H NMR spectrum was acquired (see Figure S6 and Table S4 in the Supporting Information).

Acknowledgements

This work was supported by the UK Engineering and Physical Sciences Research Council (EPSRC), the National Science Foundation (NSF/CHE-1124244) and Schlumberger-Faculty for the Future Fellowship (RAB). W.C. Isley III was supported by the Kenneth E. and Marion S. Endowed Fellowship. We thank Dr P. Mal for preliminary experimental studies and Dr M.M.J. Smulders for useful discussions.

Notes and references

^a Department of Chemistry, Chemical Theory Center, and Supercomputer Institute, University of Minnesota, 207 Pleasant St. SE, Minneapolis, MN 55455, U.S.A.

^b Department of Chemistry, University of Cambridge, Lensfield Road, Cambridge CB2 1EW, U.K.

Electronic Supplementary Information (ESI) available. See DOI: 10.1039/b000000x/

1. D. C. Crans, L. Yang, E. Gaidamauskas, R. Khan, W. Jin and U. Simonis, in *Paramagnetic Resonance of Metallobiomolecules*, American Chemical Society, 2003, pp. 304-326.
2. S. S. Rocks, W. W. Brennessel, T. E. Machonkin and P. L. Holland, *Inorg. Chim. Acta*, 2009, **362**, 1387-1390.
3. S. Turega, M. Whitehead, B. R. Hall, M. F. Haddow, C. A. Hunter and M. D. Ward, *Chem. Commun.*, 2012, **48**, 2752-2754.
4. P. S. Nadaud, J. J. Helmus, S. L. Kall and C. P. Jaroniec, *J. Am. Chem. Soc.*, 2009, **131**, 8108-8120.
5. M. Kaupp and F. H. Kohler, *Coord. Chem. Rev.*, 2009, **253**, 2376-2386.
6. M. Kruck, D. C. Sauer, M. Enders, H. Wadeplahl and L. H. Gade, *Dalton Trans.*, 2011, **40**, 10406-10415.
7. M. A. Shaibat, L. B. Casabianca, N. P. Wickramasinghe, S. Guggenheim, A. C. de Dios and Y. Ishii, *J. Am. Chem. Soc.*, 2007, **129**, 10968-10969.
8. H. Amouri, C. Desmaretz and J. Moussa, *Chem. Rev.*, 2012, **112**, 2015-2041.
9. L. Fabbrizzi and A. Poggi, *Chem. Soc. Rev.*, 2013, **42**, 1681-1699.
10. V. Amendola and L. Fabbrizzi, *Chem. Commun.*, 2009, 513-531.
11. K. Ono, M. Yoshizawa, M. Akita, T. Kato, Y. Tsunobuchi, S.-i. Ohkoshi and M. Fujita, *J. Am. Chem. Soc.*, 2009, **131**, 2782-2783.
12. J. Olguín and S. Brooker, in *Spin-Crossover Materials*, John Wiley & Sons Ltd, 2013, pp. 77-120.
13. M. A. Halcrow, *Chem. Soc. Rev.*, 2011, **40**, 4119-4142.
14. A. Bousseksou, G. Molnár, J. A. Real and K. Tanaka, *Coord. Chem. Rev.*, 2007, **251**, 1822-1833.

15. G. Aromí, L. A. Barrios, O. Roubeau and P. Gamez, *Coord. Chem. Rev.*, 2011, **255**, 485-546.
16. K. S. Murray and C. J. Kepert, in *Spin Crossover in Transition Metal Compounds I*, eds. P. Gütllich and H. A. Goodwin, Springer Berlin Heidelberg, 2004, pp. 195-228.
17. P. Gütllich and H. A. Goodwin, in *Spin Crossover in Transition Metal Compounds I*, eds. P. Gütllich and H. A. Goodwin, Springer Berlin Heidelberg, 2004, pp. 1-47.
18. J.-F. Létard, P. Guionneau and L. Goux-Capes, in *Spin Crossover in Transition Metal Compounds III*, Springer Berlin Heidelberg, 2004, pp. 221-249.
19. A. Hauser, J. Jeftić, H. Romstedt, R. Hinek and H. Spiering, *Coord. Chem. Rev.*, 1999, **190-192**, 471-491.
20. O. Kahn and C. J. Martinez, *Science*, 1998, **279**, 44-48.
21. J. A. Kitchen, J. Olguín, R. Kulmaczewski, N. G. White, V. A. Milway, G. N. L. Jameson, J. L. Tallon and S. Brooker, *Inorg. Chem.*, 2013, **52**, 11185-11199.
22. R. A. Bilbeisi, S. Zarra, H. L. Feltham, G. N. Jameson, J. K. Clegg, S. Brooker and J. R. Nitschke, *Chem. Eur. J.*, 2013, **19**, 8058-8062.
23. J. A. Kitchen, N. G. White, M. Boyd, B. Moubaraki, K. S. Murray, P. D. W. Boyd and S. Brooker, *Inorg. Chem.*, 2009, **48**, 6670-6679.
24. A. Bhattacharjee, M. Roy, V. Ksenofontov, J. A. Kitchen, S. Brooker and P. Gütllich, *Eur. J. Inorg. Chem.*, 2013, **2013**, 843-849.
25. M. G. Cowan, J. Olguín, S. Narayanaswamy, J. L. Tallon and S. Brooker, *J. Am. Chem. Soc.*, 2011, **134**, 2892-2894.
26. P. Chakraborty, M.-L. Boillot, A. Tissot and A. Hauser, *Angew. Chem. Int. Ed.*, 2013, **52**, 7139-7142.
27. P. Mal, D. Schultz, K. Beyeh, K. Rissanen and J. R. Nitschke, *Angew. Chem. Int. Ed.*, 2008, **47**, 8297-8301.
28. J. A. Wolny, H. Paulsen, A. X. Trautwein and V. Schünemann, *Coord. Chem. Rev.*, 2009, **253**, 2423-2431.
29. M. Kepenekian, V. Robert, B. Le Guennic and C. De Graaf, *J. Comput. Chem.*, 2009, **30**, 2327-2333.
30. D. N. Bowman and E. Jakubikova, *Inorg. Chem.*, 2012, **51**, 6011-6019.
31. M. Swart, *J. Chem. Theory Comput.*, 2008, **4**, 2057-2066.
32. M. Reiher, O. Salomon and B. Artur Hess, *Theor. Chem. Acc.*, 2001, **107**, 48-55.
33. A. Drogheiti, D. Alfè and S. Sanvito, *J. Chem. Phys.*, 2012, **137**, -.
34. A. Fouqueau, S. Mer, M. E. Casida, L. M. Lawson Daku, A. Hauser, T. Mineva and F. Neese, *J. Chem. Phys.*, 2004, **120**, 9473-9486.
35. R. J. Deeth and N. Fey, *J. Comput. Chem.*, 2004, **25**, 1840-1848.
36. L. M. Lawson Daku, A. Vargas, A. Hauser, A. Fouqueau and M. E. Casida, *ChemPhysChem*, 2005, **6**, 1393-1410.
37. K. P. Kepp, *Coord. Chem. Rev.*, 2013, **257**, 196-209.
38. K. Pierloot and S. Vancoillie, *J. Chem. Phys.*, 2006, **125**, 124303.
39. H. Paulsen, V. Schünemann and J. A. Wolny, *Eur. J. Inorg. Chem.*, 2013, **2013**, 628-641.
40. R. Herchel and Z. Travnicek, *Dalton Trans.*, 2013, **42**, 16279-16288.
41. B. Le Guennic, T. Floyd, B. R. Galan, J. Autschbach and J. B. Keister, *Inorg. Chem.*, 2009, **48**, 5504-5511.
42. G. Brewer, M. J. Olida, A. M. Schmiedekamp, C. Viragh and P. Y. Zavalij, *Dalton Trans.*, 2006, 5617-5629.
43. M. M. Smulders, S. Zarra and J. R. Nitschke, *J. Am. Chem. Soc.*, 2013, **135**, 7039-7046.
44. T. K. Ronson, C. Giri, N. K. Beyeh, A. Minkinen, F. Topic, J. J. Holstein, K. Rissanen and J. R. Nitschke, *Chem. Eur. J.*, 2013, **19**, 3374-3382.
45. T. B. Faust, F. Tuna, G. A. Timco, M. Affronte, V. Bellini, W. Wernsdorfer and R. E. P. Winpenny, *Dalton Trans.*, 2012, **41**, 13626-13631.
46. I. A. Riddell, M. M. Smulders, J. K. Clegg, Y. R. Hristova, B. Breiner, J. D. Thoburn and J. R. Nitschke, *Nat. Chem.*, 2012, **4**, 751-756.
47. F. Rastrelli and A. Bagno, *Chem. Eur. J.*, 2009, **15**, 7990-8004.
48. E. D. Hedegård, J. Kongsted and S. P. A. Sauer, *J. Chem. Theory Comp.*, 2013, **9**, 2380-2388.
49. J. Mao, Y. Zhang and E. Oldfield, *J. Am. Chem. Soc.*, 2002, **124**, 13911-13920.
50. W. Klauui, W. Eberspach and P. Guetlich, *Inorg. Chem.*, 1987, **26**, 3977-3982.
51. S. Grimme, S. Ehrlich and L. Goerigk, *J. Comput. Chem.*, 2011, **32**, 1456-1465.
52. R. D. Shannon, *Acta Crystallogr. Sect. A*, 1976, **32**, 751-767.
53. Y. Zhao and D. G. Truhlar, *J. Chem. Phys.*, 2006, **125**, 194101.
54. M. Dolg, U. Wedig, H. Stoll and H. Preuss, *J. Chem. Phys.*, 1987, **86**, 866-872.
55. J. M. L. Martin and A. Sundermann, *J. Chem. Phys.*, 2001, **114**, 3408-3420.
56. R. E. Easton, D. J. Giesen, A. Welch, C. J. Cramer and D. G. Truhlar, *Theor. Chim. Acta*, 1996, **93**, 281-301.
57. R. F. Ribeiro, A. V. Marenich, C. J. Cramer and D. G. Truhlar, *J. Phys. Chem. B*, 2011, **115**, 14556-14562.
58. C. J. Cramer, *Essentials of Computational Chemistry: Theories and Models*, John Wiley & Sons, Chichester, 2004.
59. G. Kervern, G. Pintacuda, Y. Zhang, E. Oldfield, C. Roukoss, E. Kuntz, E. Herdtweck, J. M. Basset, S. Cadars, A. Lesage, C. Coperet and L. Emsley, *J. Am. Chem. Soc.*, 2006, **128**, 13545-13552.
60. B. Pritchard and J. Autschbach, *Inorg. Chem.*, 2012, **51**, 8340-8351.
61. J. R. Cheeseman, G. W. Trucks, T. A. Keith and M. J. Frisch, *J. Chem. Phys.*, 1996, **104**, 5497-5509.
62. Z. Rinkevicius, J. Vaara, L. Telyatnyk and O. Vahtras, *J. Chem. Phys.*, 2003, **118**, 2550-2561.
63. A. J. H. Wachters, *J. Chem. Phys.*, 1970, **52**, 1033-1036.
64. P. J. Hay, *J. Chem. Phys.*, 1977, **66**, 4377-4384.
65. V. Barone, in *Recent Advances in Density Functional Methods, Part I*, ed. D. P. Chong, World Scientific Publ. Co., Singapore, 1996.
66. A. D. McLean and G. S. Chandler, *J. Chem. Phys.*, 1980, **72**, 5639-5648.
67. R. Krishnan, J. S. Binkley, R. Seeger and J. A. Pople, *J. Chem. Phys.*, 1980, **72**, 650-654.
68. F. Neese, *J. Chem. Phys.*, 2005, **122**, 34107.
69. M. J. Frisch, G. W. Trucks, H. B. Schlegel, G. E. Scuseria, M. A. Robb, J. R. Cheeseman, G. Scalmani, V. Barone, B. Mennucci, G. A. Petersson, H. Nakatsuji, M. Caricato, X. Li, H. P. Hratchian, A. F. Izmaylov, J. Bloino, G. Zheng, J. L. Sonnenberg, M. Hada, M. Ehara, K. Toyota, R. Fukuda, J. Hasegawa, M. Ishida, T. Nakajima, Y. Honda, O. Kitao, H. Nakai, T. Vreven, J. A. Montgomery Jr., J. E. Peralta, F. Ogliaro, M. Bearpark, J. J. Heyd, E. Brothers, K. N. Kudin, V. N. Staroverov, R. Kobayashi, J. Normand, K. Raghavachari, A. Rendell, J. C. Burant, S. S. Iyengar, J. Tomasi, M. Cossi, N. Rega, J. M. Millam, M. Klene, J. E. Knox, J. B. Cross, V. Bakken, C. Adamo, J. Jaramillo, R. Gomperts, R. E. Stratmann, O. Yazyev, A. J. Austin, R. Cammi, C. Pomelli, J. W. Ochterski, R. L. Martin, K. Morokuma, V. G. Zakrzewski, G. A. Voth, P. Salvador, J. J. Dannenberg, S. Dapprich, A. D. Daniels, F. Farkas, J. B. Foresman, J. V. Ortiz, J. Cioslowski and D. J. Fox, Gaussian Inc., Wallingford CT 2009.
70. A. V. Marenich, C. J. Cramer and D. G. Truhlar, *J. Phys. Chem. B*, 2009, **113**, 6378-6396.
71. F. Neese, *WIREs Comput. Mol. Sci.*, 2012, **2**, 73-78.